**THERMAL PROPERTIES OF CHALCOGENIDE GLASSES**

*J. David Musgraves, Sylvain Danto, and Kathleen Richardson*
*School of Materials Science and Engineering*
*Clemson University*
*Clemson, SC 29631, USA*

## 2.1 Introduction

Thermal analysis is one of the most ubiquitous set of measurement techniques in glass science, and can deliver information about glass structure and properties over a wide range of length scales and application areas. Due to the fundamental differences in chemistry between chalcogenide glasses and their oxide counterparts, the thermal behavior and response of these glass families is markedly different in many important ways. The aim of this chapter is to present a broad overview of the wide variety of thermal analysis techniques and their application to chalcogenide glasses, with a focus on the use of these glasses in hot-forming applications such as extrusion, precision glass molding, and fiber optic drawing. Sections 2.2 through 2.4 will introduce some basic principles of thermal analysis, such as differential scanning calorimetry (DSC), thermogravimetric (TGA), and thermomechanical (TMA) study of the composition dependence of properties in the sulfur, selenium and tellurium glass families. Section 2.5 opens with an overview of viscometric measurements, followed by a discussion of the important role of the viscosity-temperature curve in the hot-forming of chalcogenide glasses, and concludes with a discussion of viscometry as a tool for fundamental glass science. Section 2.6 discusses thermo-optic behavior, beginning with a description of the measurement and discussion of the impact of thermo-optic properties on device design, and ending with preliminary data on the composition dependence of this important optical design parameter. Section 2.7 will briefly suggest some future directions for the application of thermal analysis to the study of chalcogenide glasses and their various applications. The data presented in the Figures in this chapter has been compiled from a large number of literature sources using the SciGlass database [1], and as thus reflect not a single set of experiments, but the best fit of the available data

## 2.2. Differential Scanning Calorimetry (DSC)

Differential scanning calorimetry (DSC) is a thermal analysis technique that measures the heat flow into or out of a sample as a function of temperature, and is used to detect thermodynamic transitions such as glass transition, crystallization or melting. The glass sample, typically powdered in order to increase the surface area available for heat transfer, is heated in an inert sample pan and the heat flux is compared to that of an adjacent, empty, reference pan. Phase transitions are detected through the differential in heat flow supplied to the sample and reference pans; for example, the first order phase transition of crystallization is an exothermic event, meaning that less heat flow is required from the calorimeter heaters to the sample pan in order to maintain the sample and reference pans at equivalent temperatures. Thus the difference in the heat flow supplied to the reference and sample shows a maximum during the phase change from amorphous to crystalline network structure. Figure 1 shows a representative DSC trace for a multi-component chalcogenide glass, indicating the positions of the glass transition ($T_g$), crystallization onset ($T_x$), crystallization peak ($T_p$), and melting peak ($T_m$).

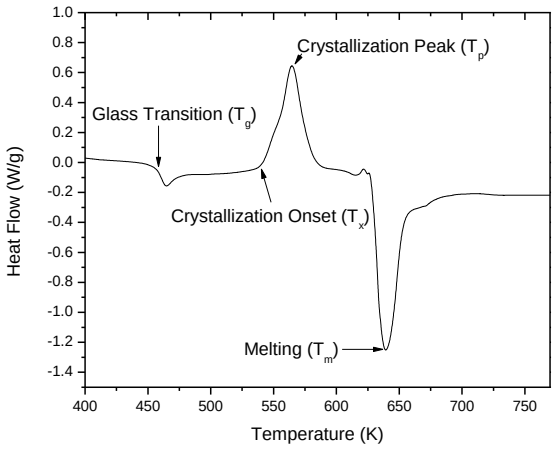


Figure 1. Example of a DSC trace for a multicomponent chalcogenide glass showing the characteristic temperatures of interest.

The glass transition, which is generally considered to be a second-order phase change [2], is visible as a slight endotherm, which may display either a minimum or merely an inflection point depending on the composition and thermal history of the glass. By comparison, the first-order thermodynamic events of crystallization and melting are visible as much larger exo- and endotherms, respectively. As will be discussed in further detail in Section 2.3, crystallization in often accompanied by volatilization of chalcogenide components, thus these measurements are made in hermetically sealed containers. For optical applications, knowledge of the temperature of the crystallization onset is more important than that of the crystallization peak, as the crystalline phases (x) formed in chalcogenides typically have a much higher refractive index (n) than that of the amorphous (a) matrix (e.g. $n(a\text{-}Ge_{50}Te_{50})$ = 3.88 vs. $n(x\text{-}Ge_{50}Te_{50})$ = 6.80 at 1550 nm) meaning that small crystal volume fractions can lead to large scattering losses in these systems [3].

**Glass transition temperature**

The glass transition is perhaps the most important thermal characteristic of an amorphous material in determining its utility in various applications, as it represents the temperature at which the material stops behaving as a rigid solid and begins to show the mechanical response of a deeply supercooled liquid, suitable for hot-forming applications. The temperature of this change in mechanical response and its relationship to the onset of melting or volatilization, discussed in Section 2.3, is critical in hot-forming applications in glasses in general, and chalcogenide glasses in particular, which tend to have much smaller working temperature ranges than oxide glasses. In addition to its utility in optical applications, the glass transition is also profoundly interesting from a fundamental science perspective. Though the existence of a glass transition is one of the defining characteristics of glass as an amorphous solid, the precise atomic-scale nature of the transition is still not completely understood [4].

To better explore some of the physical and chemical factors underlying the glass transition, the values of $T_g$ for arsenic- and germanium-based binary chalcogenide glasses are plotted in Figure 2 with the bottom axis giving the mole percent of the modifier (the As or Ge), and the top axis giving the resulting average coordination number, <r>. The average coordination number gives a measure of the mechanical constraint in the network, and is calculated for these binary systems by assuming the coordination number of Ge is 4, that of As is 3, and those of S, Se, and Te are 2 and taking the average weighted by the relative

atomic fraction of each species in a given composition. In the definition of Phillips et al., amorphous networks with a value of <r> of less than 2.4 are referred to as "floppy" (meaning they support a population of zero-frequency normal modes) [5], those with <r> greater than 2.4 are referred to as "stressed rigid"(meaning that the network is overconstrained), and those with <r> equal to 2.4 are called "isostatic"(meaning stress-free) [6]. By looking at the evolution of various properties both as a function of modifier percent and coordination number, trends which are due to chemistry (modifier) or physical constraint (coordination number) become evident.

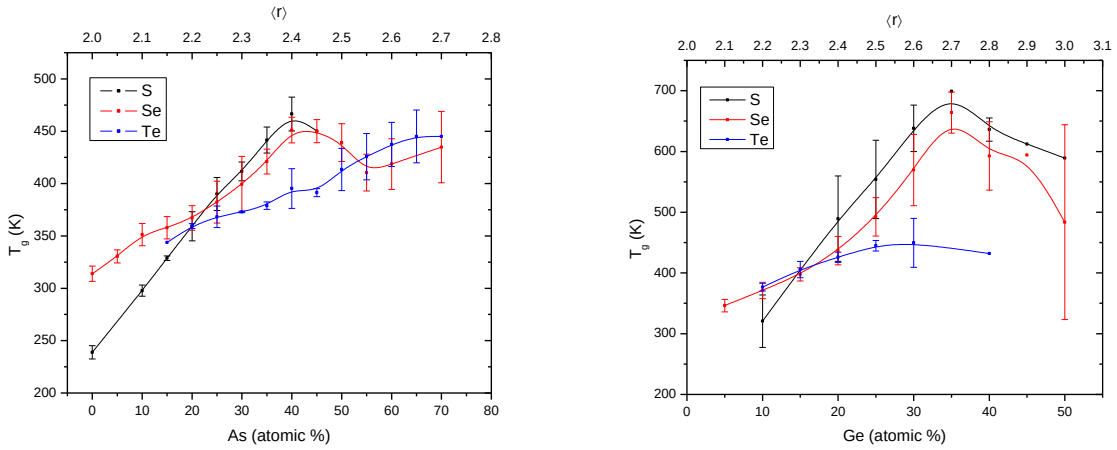


Figure 2. Variations in $T_g$ for arsenic- and germanium-based binary chalcogenide glasses.

As depicted in Figure 2, chalcogen-rich compositions show a roughly linear increase in $T_g$ as a function of modifier. In this low modifier end of the plot, the increase in $T_g$ in the Se- and Te-based glasses in each family appear to proceed at similar rates while the $T_g$ increase in the S-based glasses proceeds much more rapidly. This change in $T_g$ as a function of modifier concentration was modeled by Gibbs and DiMarzio in the context of crosslinking of polymer chains as [7, 8]:

$$(1)\quad T_g = \frac{T_0}{1-\kappa X}$$

where $X$ is the fraction of the crosslinking agent, $T_0$ is the glass transition temperature of the pure polymer chain, and $\kappa$ is a system constant. The Gibbs-DiMarzio model was developed to describe how the glass transition of long organic polymer chains (ie. rubbers, plastics, tars) varied as a function of crosslinking agent. This model was later successfully applied to chalcogenide glass systems by replacing X with the average coordination number <r> of the network [9]:

$$(2)\quad T_g = \frac{T_0}{\left[1-\beta\left(\langle r\rangle - 2\right)\right]}$$

where $\beta$ is now a system-dependant constant. This form accurately captures the linear increase in $T_g$ in the low-modifier end of the binary chalcogenides shown in Figure 2, where $\beta$ is left as a fitting parameter, which depends on the composition of the binary. Table 1 shows the best fits of Equation 2 to the low-modifier (> 20 %) data shown in Figure 2, where the values of $T_0$ for the S, Se, and Te systems are assumed to be 245, 316, and 343 K, respectively [10].

Table 1. Best-fit values of β from Equation 2 to the low-modifier (> 20 %) data in Figure 2

| Glass System | Best-Fit β |
|---|---|
| AsS | 1.679 |
| AsSe | 0.739 |
| AsTe | 0.272 |
| GeS | 1.029 |
| GeSe | 0.752 |
| GeTe | 0.476 |

Interestingly, β is more strongly impacted by the identity of the chalcogen (compare 1.679 to 0.272 for AsS to AsTe) than that of the modifier (compare 0.739 to 0.752 for AsSe to GeSe). As may have been expected, the change in the glass transition behavior of the binary chalcogenide glasses is dominated more by the network (chalcogen) than the modifier (As or Ge) in the low-modifier range of the composition space.

Stochastic Agglomeration Theory attempts, in small part, to derive an analytical expression for β in order to express this constant in terms of more fundamental, network-oriented considerations, namely the coordination number of each atom in the chalcogenide binary [10]:

$$(3)\quad \frac{1}{\beta} = \left(m' - m\right)\ln\left(\frac{m'}{m}\right)$$

where *m* is the coordination number of the chalcogen (ie. 2) and *m'* is the coordination number of the modifier (3 for As and 4 for Ge). This expression was arrived at by "solving" Equation 2 for β, and expressing the average coordination number, <r>, as a function of the coordination of the network, *m*, and the modifier, *m'*. The model predicts a β value of 2.466 for the As-based system and 0.721 for the Ge-based system, which is reasonably close to that shown in Table 1 for the GeSe system; clearly though, this simple relationship linking the system-dependent β parameter to only mechanical constraints in the network has not captured the evolution of β with the chalcogen type, which indicates that there are additional contributions due to the chemistry of the system that have not been accounted for.

Returning to the trends shown in Figure 2, the S- and Se-based glasses in both families exhibit maxima in the glass transition temperature at the stoichiometric compositions: $As_{40}X_{60}$ and $Ge_{33.33}X_{66.66}$ for X=S and Se. In both families there is much less evidence for a clear maximum in variation in $T_g$ with modifier concentration in the Te-based glasses. These maxima in the S and Se binaries occur at <r> = 2.4 and 2.7 for the As and Ge systems, respectively. Much has been made of the occurrence of the maximum of the glass transition temperature for the AsS and AsSe systems at an average network coordination of 2.4, which is directly in line with the transition from a floppy to stressed-rigid network according to Constraint Theory [11, 12]. However, the shift of this maximum to an average network coordination of 2.7 in the GeS and GeSe compositions, above even the "intermediate phase" of network structures [13, 14], suggests that this maximum is not strictly determined by network mechanics, but by system chemistry as well. Some composition regions show clear evidence of nanoscale phase separation, which could affect the effective average coordination number of the network and put it more in line with the trends shown in Figure 2, but the exact structural nature of these nanoscale phases is still a topic of debate in chalcogenide glasses [15, 16].

The same maxima shown in the glass transition temperatures of the binary sulfur and selenium glasses are evident in more complicated glass forming systems based on these elements, as shown in Figure 3, which illustrates the variation in $T_g$ in the As-Ge-S and As-Ge-Se glass forming regions of composition space.

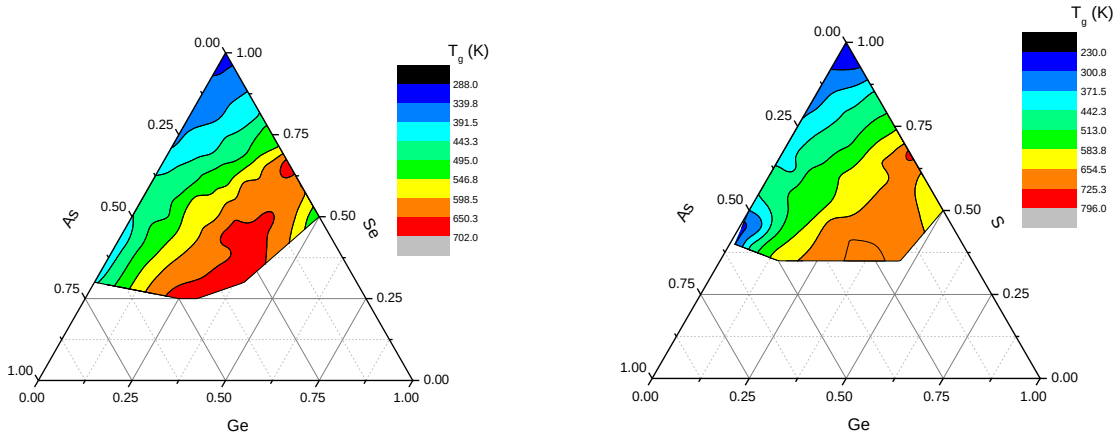


Figure 3. Variations in $T_g$ for As-Ge(S,Se) ternary chalcogenide glasses.

The authors know of no published model which accurately captures the complexity of the variation in $T_g$ with composition in these ternary systems. Small pockets of elevated $T_g$ in composition space may indicate the presence of the nanoscale phase separation described above. The texture of the contours of $T_g$ variation themselves are interesting in that they are not nearly as regular as those shown by variations in other properties such as the coefficient of thermal expansion (see Figure 7).

**Crystallization stability**

Crystallization stability, defined as the distance in temperature space between the glass transition and the onset of crystallization (ie. $\Delta T = T_x - T_g$), determines the suitability of a given chalcogenide glass composition for various hot-forming applications. Stability towards crystallization in hot-forming processes represents a balance between the need to deform the glass, which must be above its glass transition temperature in order to flow, and the need to retain a crystal-free network in order to maintain the optical properties and shaping amenability of the amorphous material. A typical 'rule of thumb' suggests a minimum $\Delta T$ of 100 K is needed to provide a sufficient temperature window for applications such as fiber drawing, and as such, multi-component systems which show a lower propensity for crystallization are of special interest. It is possible to form chalcogenide glasses with $\Delta T$ less than 100 K, however these typically require extreme forming procedures to prevent crystallization of the network [17]. Table 2 shows the evolution of the crystallization stability window as a function of composition in a four-component series of glasses as the chalcogen is gradually changed from sulfur to selenium [18].

Table 2. Glass transition and crystallization temperatures, with corresponding stability windows, for two families of chalcogenide glasses.

| Composition | $T_g$ (K) [±2 K] | $T_x$(K) [±2 K] | $\Delta T = T_x - T_g$ |
|---|---|---|---|
| $Ge_{28}Sb_{12}Se_{60}$ | 615 | 800 | 185 |
| $Ge_{28}Sb_{12}S_{45}Se_{15}$ | 596 | 784 | 188 |
| $Ge_{28}Sb_{12}S_{30}Se_{30}$ | 592 | 766 | 174 |
| $Ge_{28}Sb_{12}S_{15}Se_{45}$ | 595 | 770 | 175 |
| $Ge_{28}Sb_{12}Se_{60}$ | 571 | 764 | 194 |
| $Ge_{28}As_{12}Se_{60}$ | 678 | 798 | 120 |
| $Ge_{28}As_{12}S_{45}Se_{15}$ | 660 | 789 | 129 |
| $Ge_{28}As_{12}S_{30}Se_{30}$ | 651 | 784 | 134 |
| $Ge_{28}As_{12}S_{15}Se_{45}$ | 649 | 782 | 133 |
| $Ge_{28}As_{12}Se_{60}$ | 615 | 778 | 163 |

Two systems are shown in Table 2, $Ge_{28}Sb_{12}S_xSe_{60-x}$ and $Ge_{28}As_{12}S_xSe_{60-x}$, where only the nature of one of the modifying elements has been changed (Sb to As). As both modifiers are threefold coordinated, any discrepancies between the two systems should be considered as chemical rather than configurational in nature. Though the glass transition temperatures of the antimonide system are lower than those measured in the arsenide system, the antimonide system exhibits a 44 K decrease in $T_g$ and a 36 K decrease in $T_x$ with selenium substitution for sulfur, while the arsenide system exhibits a 63 K decrease in $T_g$ and an 11 K decrease in $T_x$ with the same substitution. These factors combine to give an increasing stability window in both systems with increasing selenium content; however the antimonide has a higher ΔT for a given sulfur/selenium ratio than the arsenide system.

**Heat capacity**

The heat capacity of a glass is a measure of the amount of thermal energy, q, required to raise the temperature of the material by 1 K. Thermal energy is converted into normal mode vibrations in the glass network, and the connectivity of the network can be expected to contribute strongly to the measured heat capacity of the glass. Heat capacity is typically measured in ambient laboratory environment using DSC, thus the reported heat capacity is the one measured at a given pressure (ie $C_p$). The heat capacity is calculated as the change in thermal energy delivered by the DSC to the sample over the change in temperature of the system:

$$C_p = \left(\frac{\partial H}{\partial T}\right)_p \approx \frac{q_p}{\Delta T} \quad (4)$$

where the constant pressure heat capacity is defined in thermodynamics as the partial derivative of the enthalpy, *H*, with respect to temperature at a constant pressure. As enthalpy is a direct measure of heat flow at constant pressure, this can be rewritten as $q_p$, which is the term measured directly by the DSC.

As it is a reflection of the underlying phonon density of states, the heat capacity of chalcogenide glass, just as any other material, is a function of temperature. Constant pressure heat capacity of a chalcogenide glass exhibits a global maximum in the glass transition range as configurational changes, including structural relaxation, contribute to the heat capacity in this temperature range in addition to the simple vibrational modes discussed above. Below and above the glass transition region, the heat capacity is a weak function of temperature in chalcogenide glasses [19]. To appropriately asses its variation as a function of composition, the heat capacity of two families of glasses below their respective glass transition temperatures is shown in Figure 4.

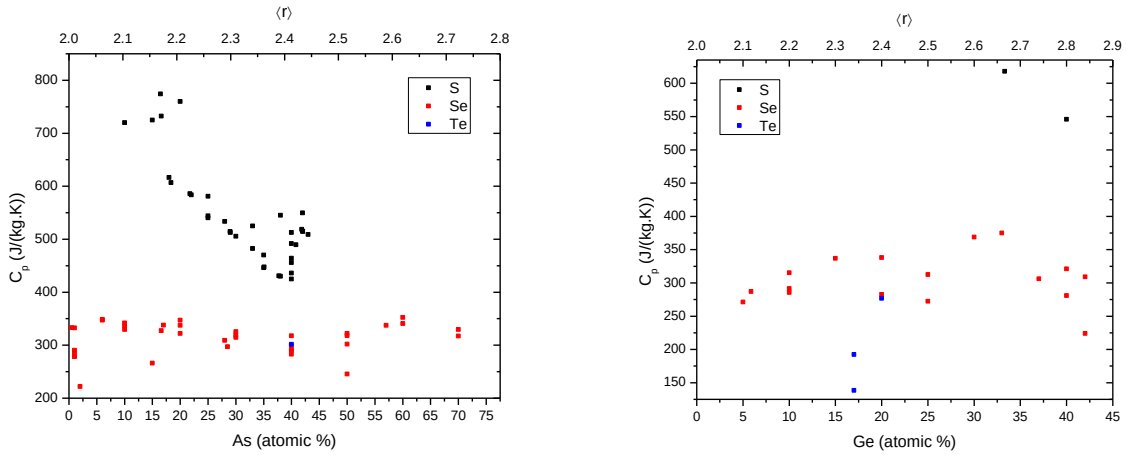


Figure 4. Variations in $C_p$ for arsenic- and germanium-based binary chalcogenide glasses.

For both the arsenic- and germanium-modified systems, the heat capacity of the (As,Ge)-Se binary is approximately 300 J/kg.K, regardless of modifier concentration, or alternatively, network constraint. This same phenomenon is exhibited in oxide glasses as well, with the heat capacity of simple soda-lime silicates measuring approximately 900 J/kgK, with very weak dependence on modifier concentration [20]. This observation in the selenide glasses is in stark contrast to that exhibited by the As-S system, which exhibits a clear decrease in sub-$T_g$ heat capacity with increasing arsenic content. However, this apparent trend is an artifact of the units in which the heat capacity is presented: the standard units, J/kgK, do not account for variation in the molar mass of the glass as a function of arsenic content; a more suitable measure for the heat capacity would be to present it as a molar unit, ie J/mol.K. The molar volume of the germanium- and arsenic-selenide glass series is a much weaker function of modifier concentration than that exhibited by the arsenic sulfide series; the molar volume varies from approximately 78.9 to 77.4 g/mol in the arsenic selenides as x varies from 0 to 40, but over the same modifier range, the molar volume changes from 31.6 to 49.2 g/mol in the sulfide system, which gives rise to the apparent variation in heat capacity shown above.

**2.3 Thermogravimetric Analysis (TGA)**

Thermogravimetric analysis (TGA) measures the mass of a glass sample as a function of temperature. In the context of hot-forming applications, this tool is critical in defining the safe upper working temperature of a given composition (here 'safe' means both safety for the experimentalist as well as safety of the fidelity of the original composition). While the crystallization stability window $\Delta T = T_x - T_g$ defines a thermodynamically suitable temperature range, it does not account for the possibility (very high in some compositions) of the glass out-gassing at temperatures above $T_g$ but below $T_x$, precisely in the working range for forming applications. Figure 5 shows a comparison of the viscosity and weight-loss profiles of the ternary chalcogenide glass $Ge_{10}As_{40}Se_{50}$. The dashed lines indicate the viscosity range ($10^6$-$10^8$ Pa.s) necessary for molding or extrusion of the chalcogenide glass, with the associated temperature range (573-628 K). As this figure indicates, by the temperature at which the glass is moldable, there is a non-zero volatilization of glass materials. This change in composition is unacceptable from both a technological and safety perspective since it will affect the refractive index of the material, and the volatilized components can be hazardous to humans.

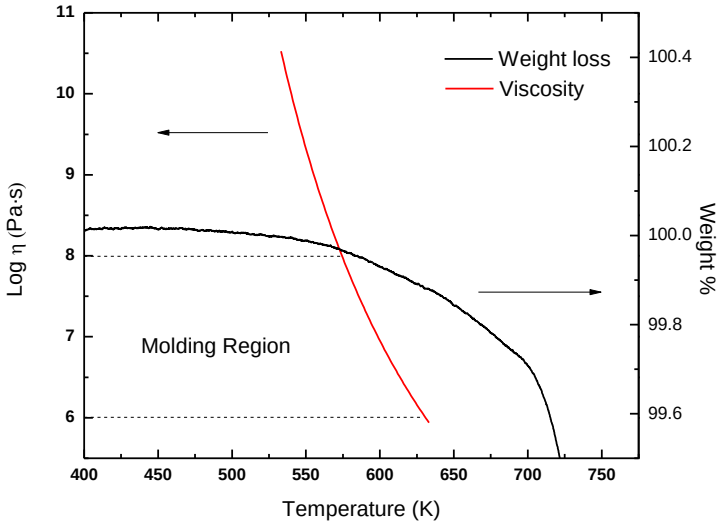


Figure 5. A comparison of the viscosity and volatilization curves for $Ge_{10}As_{40}Se_{50}$ glass showing evidence of out-gassing in the molding region.

If one assumes a maximum tolerable volatilization level of 0.2 weight percent for a given application, the TGA can be used to provide safe working ranges for the hot-forming of chalcogenide glasses. Table 3 shows a comparison of the glass transition temperature and temperature of 0.2 % weight loss for some commercially available chalcogenide glass compositions as determined by TGA measurements made in the authors' laboratory. The heating rate for the glass transition measurement was 10 K/min, and that used for the weight loss measurements was 1 K/min, in both cases the samples consisted of 10-30 mg of powdered glass. Based on these values, a suggested 'safe' working range for each glass is shown at the right of the table. It should be noted that this definition of 'safe working range' is ours as defined here, but will vary depending on application and specific laboratory safety considerations and guidelines.

Table 3. Glass transitions, and 0.2 % weight loss temperatures for some commercially available chalcogenide glasses.

| **Composition** | **$T_g$ (K)** | **$T_{0.2\%}$ (K)** | **Safe working range (K)** |
|---|---|---|---|
| $Ge_{33}As_{12}Se_{55}$ | 611 | 726 | 115 |
| $Ge_{30}As_{13}Se_{32}Te_{25}$ | 565 | 752 | 187 |
| $Ge_{10}As_{40}Se_{50}$ | 516 | 667 | 151 |
| $Ge_{28}Sb_{12}Se_{60}$ | 576 | 757 | 181 |
| $As_{40}Se_{60}$ | 468 | 621 | 153 |

The largest safe working ranges belong to the $Ge_{30}As_{13}Se_{32}Te_{25}$ and $Ge_{28}Sb_{12}Se_{60}$ compositions, due to their structure containing the heavier (and more difficult to volatilize) Sb and Te elements. The next widest working ranges are exhibited by the $Ge_{10}As_{40}Se_{50}$ and $As_{40}Se_{60}$, indicating that low levels of Ge do not significantly impact the volatilization tendency of the arsenic selenide glass family. The lowest safe working range is shown by the $Ge_{33}As_{12}Se_{55}$ composition, not because its 0.2% weight loss temperature is lower, but because of its comparatively high $T_g$. Note that these safe working ranges are not identical to the crystallization stability window, $\Delta T$, for a given glass, and indeed the change in composition may be triggered by the onset of crystallization or vice versa.

**2.4 Thermomechanical Analysis (TMA)**

Thermomechanical analysis (TMA) provides information on the mechanical response of a glass sample to an applied thermal load. Measurement of the expansion or contraction of a glass composition as a function of temperature can be conducted with either a TMA instrument, which operates in a vertical geometry, or a dilatometer, which operates horizontally. In either case, a silica pushrod is placed in contact with one face of the glass sample, and the movement of this pushrod is measured with a linear variable differential transformer (LVDT).

The coefficient of thermal expansion, or CTE, is a measure of the mechanical response of a glass network to an applied thermal load. The linear expansion of a system in response to an increase in temperature is thus written as

(5) $$dL = \alpha_L L dT \text{ or } \alpha_L = \frac{1}{L}\frac{dL}{dT}$$

where *L* is the length of the sample at room temperature, *dL* is the change in length, *dT* is the change in temperature and $\alpha_L$ is the linear CTE. Because the CTE measurements are typically performed below the glass transition temperature, there is no contribution to the thermal expansion from conformation or bonding changes in the material; the expansion is a reflection of the aggregate change in interatomic bonding distances. In general, as the temperature of a glass is increased in the region below $T_g$, the additional thermal energy permits the elongation of the mean bond length as dictated by the shape of the potential energy well representing the bond[21].

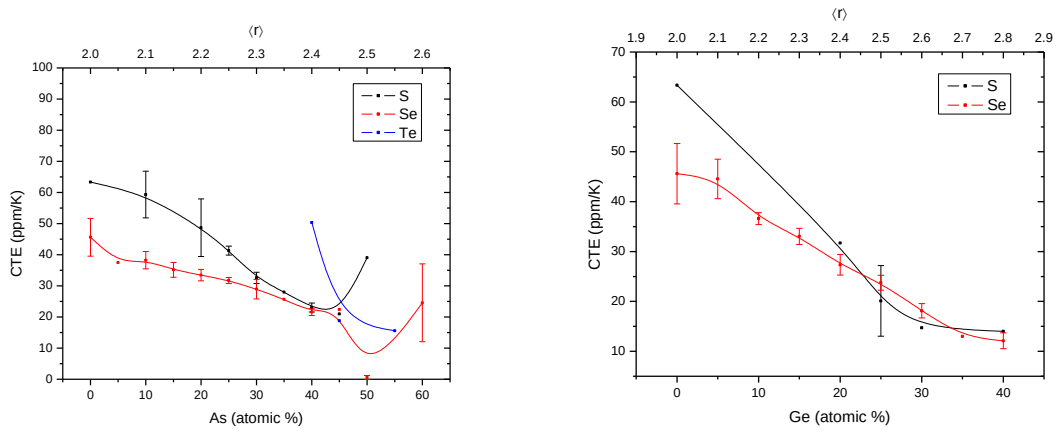


Figure 6. Variations in CTE for arsenic- and germanium-based binary chalcogenide glasses.

As shown in Figure 6, in the arsenic system, the evolution of the measured CTE with As % follows a almost linear trend win both the sulfur and the selenium based systems, with an apparent local minimum at the stoicheometric $As_{40}S_{60}$ (<r> = 2.4) composition, and a similar local minimum at the slightly arsenic rich composition of $As_{50}Se_{50}$. Following these minima, the linear trend is no longer evident, as the CTE begins to rise with increasing arsenic content before leaving the glass forming region.

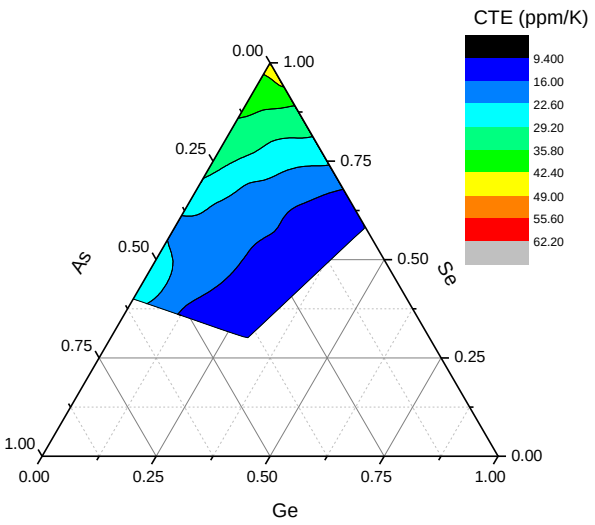


Figure 7. Variations in CTE for As-Ge-Se ternary chalcogenide glasses.

This minimum in the CTE in the arsenic selenide series, as well as the seeming lack of minimum in the germanium selenide series, can be seen together in Figure 7. The regularly-banded contours of the CTE variation, indicative of a property which exhibits an orderly variation as a function of composition, are interrupted by a brief excursion where the 20 ppm/K band pushes out to meet the As-Se binary tie line. That this minimum occurs where the arsenic selenide system is overconstrained (<r> = 2.5) suggests nanoscale phase separation may be occurring in these systems.

**2.5 Viscometry**

Knowledge of the viscosity of chalcogenide glasses at a given temperature is one of the most fundamental concerns in the formation and processing of these materials. Possibly even more critical than the value of the glass transition temperature, $T_g$, as the glass transition can be estimated from the viscosity curve. The viscoelastic behavior of a glass is critical in all hot-forming processes, as it dictates the time and temperature scales needed to precisely produce optical elements, from slow, low-temperature extrusion to rapid, high-temperature fiber drawing. Aside from its technological importance, the viscosity-temperature relationship has significant value from the perspective of fundamental research into the connections between the atomic structure of amorphous solids and the properties that result from this structural arrangement.

**2.5.1 Techniques**

A wide variety of viscometric techniques are used in industrial and academic glass science due to the wide range of viscosities exhibited by a glass as a function of temperature. Viscosity of chalcogenide glasses changes over 17 orders of magnitude in less than 500 K, meaning the viscosity ranges appropriate for various hot-forming methods may only be accessible in small ( < 50 K) temperature windows. Some of these forming regions, as well as an overview of some of the viscometric techniques used are shown in Figure 8. Each measurement technique requires a different sample geometry, some with precise tolerances and others without, and as with many measurements, the quality of the sample dramatically impacts the accuracy of the data obtained. Data from multiple viscometric techniques combined to generate a viscosity-temperature curve for a given material, such as that shown in Figures 8 and 10.

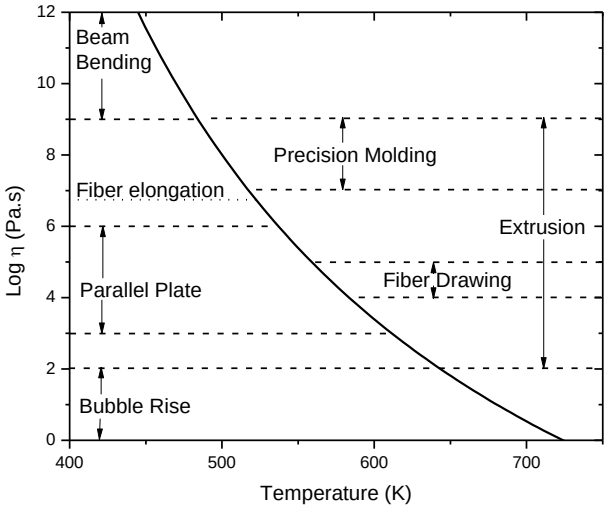


Figure 8. An overview of the viscosity regions for a chalcogenide glass, showing the ranges for measurements (left) and hot-forming applications (right).

**Parallel Plate Viscometry**

Parallel plate viscometry is used to probe the viscosity of a glass in the range of $10^3$ – $10^6$ Pa.s, where the glass is behaving as a viscous supercooled liquid rather than a solid in terms of flow. A right cylinder of the glass is compressed under load at temperature between two parallel plates. From the compression rate, the viscosity of the glass can be calculated using [22]:

$$\eta = 2\pi \frac{Mgh^5}{30V\left(dh/dt\right)\left(2\pi h^5 + V\right)\left(1+\alpha T\right)} \quad (6)$$

where $\eta$ is the viscosity in Pa.s, $M$ is the applied load, g is the acceleration due to gravity, $h$ is the sample height at time $t$, $V$ is the sample volume, $dh/dt$ is the compression rate, and $\alpha$ is the CTE of the glass.

**Beam Bending Viscometry**

Beam bending viscometry probes the viscosity of a glass in the range of $10^9$ to $10^{13}$ Pa.s, where the glass's flow behavior resembles that of a solid rather than a viscous liquid. The temperature at which the viscosity is equal to $10^{12}$ Pa.s is typically equated to the glass transition, $T_g$, though this is largely an empirical convention rather than a thermodynamic or kinetic distinction. Beam bending viscometry measures the deflection of a beam of glass under load at a defined temperature using a linear variable differential transformer (LVDT). From this deflection, the viscosity of the glass at temperature T can be calculated using [23]:

$$\eta = \frac{gL^3}{1440 I_c \frac{dh}{dt}}\left[\frac{M+\left(\rho AL\right)}{1.6}\right]\left[\frac{\left(1+\alpha_s T\right)^3}{\left(1+\alpha_g T\right)^4}\right] \quad (7)$$

where $\eta$ is the viscosity in Pa.s, g is the acceleration due to gravity, $L$ is the support span, $I_c$ is the cross sectional moment of inertia, $dh/dt$ is the deflection rate, $M$ is the applied load, $\rho$ is the glass density, $A$ is

the cross sectional area of the beam, $\alpha_s$ is the coefficient of thermal expansion (CTE) of the support stand and $\alpha_g$ is the CTE of the test glass.

**Fiber elongation**

Fiber elongation is a viscometric technique used to measure intermediate viscosities, between those probed by the beam bending and parallel plate methods described above. In particular, the fiber elongation technique can be used to precisely calculate the Littleton softening temperature of the glass, where the viscosity is defined as $\eta = 10^{6.6}$ Pa.s [24]. Knowledge of the Littleton softening temperature is critical in the analysis of fiber drawing parameters for chalcogenide glasses, as it describes the temperature at which a glass fiber will deform under its own weight. This viscosity/temperature value is measured by observing the rate of deflection of a sample fiber contained in a furnace. The viscosity can be calculated from this deflection rate using:

$$\eta = \frac{\left(Lp + \frac{p^2}{2}\right)\rho g - \frac{\gamma p}{r}}{3\frac{dp}{dt}} \quad (8)$$

where $\eta$ is the viscosity of the glass in Pa.s, $L$ is the length of fiber outside of the furnace, $p$ is the length of fiber inside the furnace, $\rho$ is the glass density, g is the acceleration due to gravity, $\gamma$ is the surface tension of the glass, and $dp/dt$ is the elongation rate of the fiber.

**2.5.2 Applications**

The right-hand side of Figure 8 shows the viscosity ranges for several hot-forming methods commonly used to shape chalcogenide glasses: extrusion, precision glass molding (PGM), and the drawing of optical fibers from bulk chalcogenide glass performs. Extrusion is the most versatile of these techniques in terms of total possible viscosity range covered by a single technique. However, different applications (ie. different geometries) require different extrusion viscosities in order to achieve optimal device performance; extrusion can be used to form glass with a viscosity like that of a soft solid being forced through a die ($10^9$ Pa.s), or like that of a viscous liquid being forced into a channel ($10^2$ Pa.s). PGM covers the next widest viscosity range of the three techniques, and is a process for molding precision chalcogenide optical lenses while the glass has the viscosity of a slightly softened solid ($10^7$-$10^9$ Pa.s). Drawing optical fiber from chalcogenide glasses requires a viscosity below that of the Littleton softening point ($10^{6.6}$ Pa.s) where a glass fiber would deform under its own weight, and is typically done in the viscosity range around $10^5$ Pa.s. Each of these techniques is used to obtain precise geometries, dimensions, and surface characteristics by taking advantage of some portion of the wide range of viscosities chalcogenide glasses exhibit in comparatively (to oxides) short temperature windows.

**Extrusion**

The extrusion of chalcogenide glasses is in many ways no different than the extrusion of polymers: a viscoelastic material is forced into a channel or through a die to form a desired geometry, then the material is cooled back below is glass transition to “lock in” the solid structure. Depending on the desired viscosity (extrusion can be used to form glasses with viscosities from $10^2$ to $10^9$ Pa.s), there may or may not be danger of volatilization of the chalcogenide glass during processing; in the high viscosity region glass can be extruded only 25-50 K above their glass transition temperature. The high CTE of chalcogenide glasses can present challenges in the extrusion of precise geometries. The prediction of the precise volume loss as the material contracts after leaving the hot-forming region is extremely difficult, but efforts are underway using computing techniques such as Finite Element Analysis to simulate the thermal response

of chalcogenide glasses in order to define accurate die geometries to obtain a desired final piece geometry. For low viscosity extrusions, there is a risk of crystallizing the glass during processing, which would undermine its shaping ability and the use of the glass in optical applications due scattering or high index contrast between the two phases.

Extrusion is increasingly used as a tool to produce preform pieces from which to draw microstructured optical fibers, as complex geometries can be extruded that may not be accessible through drilling, stack and draw, or other structure-forming methods [25-27]. In addition to the production of more complex geometries, extrusion can also be used to produce pieces or preforms from complicated material combinations such as chalcogenide glasses paired with oxide glasses, polymers, or metals. An example of such a combination is shown in Figure 9 [28].

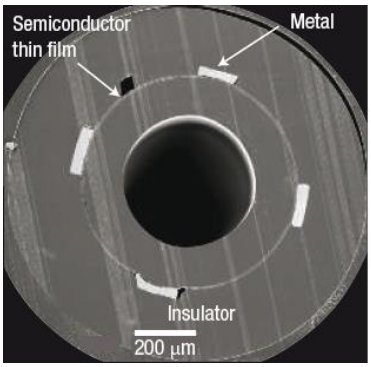


Figure 9. Cross-section of a microstructured optical fiber incorporating chalcogenide glass film, polymeric cladding and metallic electrodes .

When drawn into a fiber, the structure in Figure 9 acts as a one dimensional photodetector. The insulator material is a polymer, the semiconductor thin film is $As_{40}Se_{60}$ glass, and the metal is tin; if an electrical voltage is applied across the metal electrodes, then an incident photon will excite a charge carrier in the $As_{40}Se_{60}$ glass, which will then register as an increase in current measured in the fiber.

**Precision Glass Molding**

Extensive growth of opto-electronic technologies has created a demand for high quality chalcogenide lenses and has driven the industry toward an inexpensive process for manufacturing of aspheric glass lenses called Precision Glass Molding (PGM). In addition PGM can achieve more complicated optical element shapes than typically realized via conventional (grinding and polishing) fabrication techniques and where single point diamond turning (SPDT) cannot be employed. Aspheric lenses are rapidly replacing spherical lenses in many high-end optical applications, as they eliminate spherical aberrations in the focal element, and quite often, reduce weight. This is especially important in infrared (IR) optical systems where elements are made from high index (high density and weight) materials. PGM is already extensively used to mold oxide glasses and polymers, which have a much shallower viscosity/temperature dependence than chalcogenides, and do not present the same volatilization dangers discussed in Section 2.3

In the PGM process the glass preform, often a precision (mass) gob or with a spherical surface of similar deviation, is raised above its $T_g$ to a viscosity of $10^7$-$10^9$ Pa.s, pressed between two mold surfaces to form the desired geometry, then cooled rapidly back to a solid. A schematic of the heating and pressing process for a chalcogenide lens is shown in Figure 10. After soaking at temperature for 240 s, the chalcogenide is pliant enough to be deformed from its original to its final, desired geometry. Because this is intended to

be a single-step process, particular care is given to the surfaces of the molds, which are typically made from a high temperature ceramic such as silicon- or tungsten-nitride. These mold surfaces must remain optically polished , which will be imparted to the chalcogenide lens during the pressing cycle. A major challenge in the pressing of chalcogenide aspheres is preventing sticking between the glass and the mold surface, for which specialized coatings have been developed which serve as an effective barrier to sticking without contaminating the surface of the precision lens [29, 30].

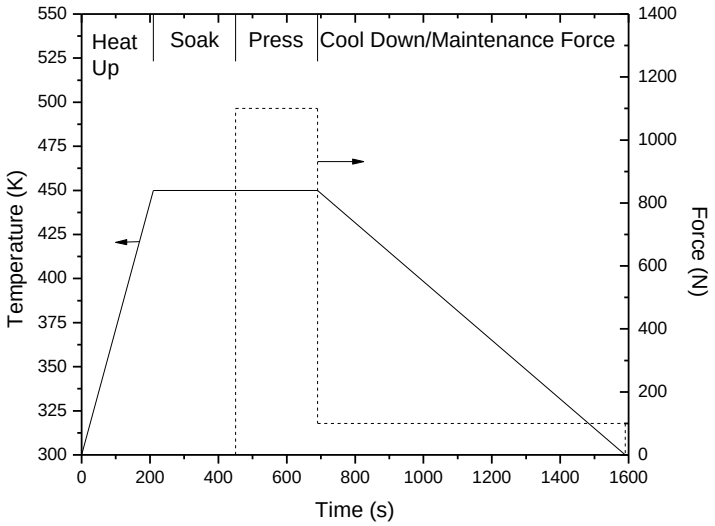


Figure 10. The temperature and force schedule for the precision molding of a chalcogenide glass.

Precision molding of chalcogenide glasses is non-trivial using the scheme shown in Figure 10 because their thermal properties are much different than those of oxide glasses. For example, the CTE of chalcogenide glasses, discussed in Section 2.4, are much higher than those of visible-optics oxide glasses; an arsenic sulfide lens can have a CTE of 60 ppm/K, as compared to 7.1 ppm/K for commercially available Schott N-BK7 glass. This CTE difference means that the chalcogenide will contract a greater volume during the cool down period than an oxide glass would, and compensations for this change in volume need to be built into the mold geometry. Low thermal conductivity and steep viscosity curve for chalcogenide glasses bring another layer of difficulty, which make precise control of the temperature of the molding system and the glass critical to achieving good parts [31-34]. Thus, to efficiently determine an optimized thermal cycle for a new candidate optical design (component material and shape), it is necessary to employ computational techniques which include contributions due to these various properties along with relaxation properties (structural and stress).

**Fiber optic drawing**

To date, determination of the forming regions (for both PGM and fiber drawing) for a new chalcogenide glass type has been done using empirical, rather than deterministic methods. Recently, researchers have made large advances in prediction of these thermal regimes using numerical modeling methods [35]. Drawing down a preform of chalcogenide glass to form an optical fiber requires raising the preform's temperature to as much as 100 K or more above its glass transition temperature in order for the glass to flow sufficiently easily ($\eta = 10^5$ Pa.s) allowing it to be pulled to a diameter up to 1000 times smaller than that of the starting bulk. As described in Section 2.3, the volatilization temperature of some chalcogenide compositions, including $Ge_{33}As_{12}Se_{55}$, can be approximately 100 K higher than $T_g$, so care must be taken

to prevent out-gassing of the glass, which would detrimentally change the composition, and could be harmful to humans. Because the viscosity curves of chalcogenide glasses are so much steeper than those of most oxides, the temperature window at which the glass is near a viscosity of $10^5$ Pa.s is comparatively smaller, thus precise temperature control is critical in drawing chalcogenides. The crystallization stability window, ΔT discussed in Section 2.2, of a given chalcogenide glass can also limit the available composition options; a $Ge_{20}Te_{80}$ composition may be quenched into an amorphous preform bulk [36], but when it is heated to the draw temperature, it will crystallize completely.

Despite the limitations, chalcogenide glasses have found great success in the application field of fiber optics. Photonic crystal fibers have been demonstrated in chalcogenide glasses [26], which show potential for novel optical properties such as dispersion tailoring [37], supercontinuum generation [38], and single-mode infrared guidance [39]. Figure 11 shows a photonic crystal fiber formed from $Ga_5Ge_{20}Sb_{10}S_{65}$ glass. The photonic crystal formed by the holes in the structure effectively guide light through the solid core. The high refractive index of chalcogenide glasses improves the confinement of the guided light, and guiding losses have been demonstrated in the range of 5 dB/km at 1.5 μm [25, 40].

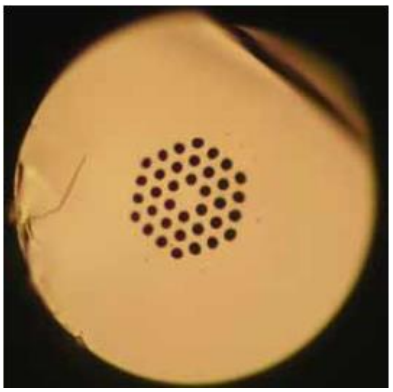

Figure 11. A photonic crystal fiber formed from $Ga_5Ge_{20}Sb_{10}S_{65}$ glass.

The high optical nonlinearity of chalcogenide glasses is being used in the development of all-optical switching, Raman gain, and infrared signal regeneration applications [41-43]. These nonlinear properties also contribute to the photosensitivity exhibited by chalcogenide glasses, which has been utilized to write waveguides and Bragg gratings into these materials. [44] In many ways, fibers take the best advantage of many of the novel optical properties that define the chalcogenide glasses, as they present a long optical path length over which the nonlinear properties can have the greatest impact.
Recently a new preform-based fiber processing technique has emerged that allows the simultaneous drawing of chalcogenide glasses in combination with metallic electrodes and polymers into tens-of-meters long structures [45]. The incorporation of materials with vastly disparate optical and electrical properties in fibers expends the traditional functionalities of the later ones from optic to acoustic [46], opto-electronic [47] or electronic [48].

### 2.5.3 Fundamental Science

In addition to the important role of viscosity in the hot-forming applications discussed in 2.5.2 scientific study of the viscoelastic behavior of glasses gives powerful insight into the atomic-level structure of amorphous networks. For example, the dimensionality, or connectedness, of an amorphous network of atoms has a direct impact on the viscous flow behavior exhibited by bulk glass: a network composed of

intertwined chains of atoms will flow differently than a network composed of sheets or clusters of atoms. Understanding how the viscosity behavior of a glass family evolves with variations in composition can shed light on the underlying network structures and dynamics that give rise to that behavior. The viscosity of the supercooled liquids in the AsS and AsSe families are shown in Figure 12. Again, these data represent a compilation of literature values obtained through the SciGlass database [1].

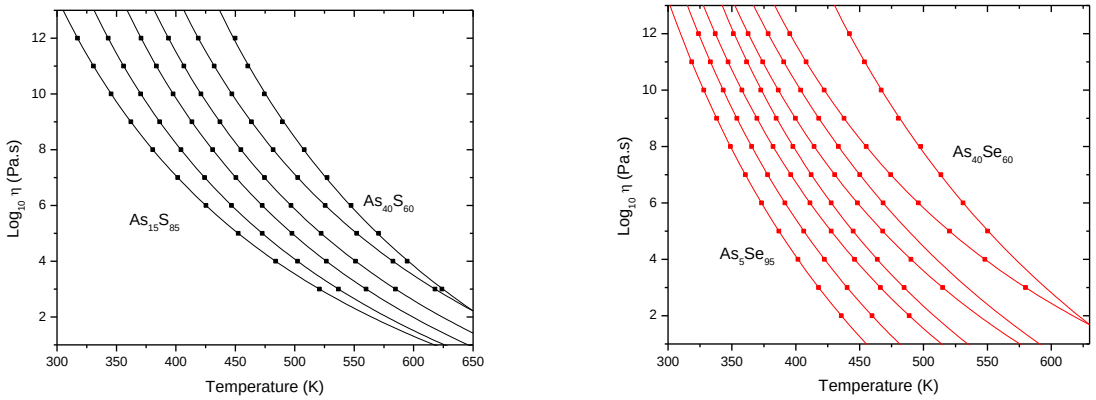


Figure 12. The temperature-viscosity dependence of the AsS and AsSe glass families

The available data for each composition has been fit using the empirical model developed by Vogel, Fulcher, and Tamann (known as the VFT model) [49]. The VFT model employs three fitting parameters (A, B, and C in Equation 9 below) to capture the curvature of the viscosity-temperature dependence; Note that while there exist modifications to this simple model, they serve mainly to improve the quality of the extrapolation of the fit to extremely high and low viscosity regimes [50].

$$log_{10}\eta = A + \frac{B}{T - C} \tag{9}$$

The change in the viscosity-temperature behavior as a function of composition of the chalcogenide glasses in Figure 12 can be evaluated using the fragility parameter, as expressed in Equation 10. The fragility parameter is a measure of the steepness of the viscosity curve, and is defined as the slope of the curve evaluated at the temperature at which the viscosity is equal to $10^{12}$ Pa s, $T_{12}$, which is commonly equated to the glass transition temperature, $T_g$, of the glass [51]:

$$m \equiv \left. \frac{\partial\left(\log_{10}\eta\right)}{\partial\left(\frac{T_{12}}{T}\right)} \right|_{T=T_{12}} = \frac{BT_g}{\left(T_g - C\right)^2} \tag{10}$$

The right-hand side of Equation 10 shows the evaluation of the fragility parameter when the VFT formalism of Equation 9 is employed, with B and C taken from the VFT expression. The fragility parameter represents how far from a purely Arrhenius description the viscosity of a glass is: silica, the prototypical Arrhenius glass has a fragility of 17, while more "fragile" polymeric glass formers have a fragility parameter near 200, meaning that their behavior is not properly described by the simple single exponential decay

of the Arrhenius function [52, 53]. Chalcogenide glasses have been shown to possess "intermediate" behavior, with fragility parameters typically between 20 and 40, much closer to that of the highly crosslinked silica network than to that of a fragile glassy polymer.

Using Equation 9 to fit the data in Figure 12, the fragility parameter can be calculated for these two families of chalcogenide glasses; these results are shown in Figure 13.

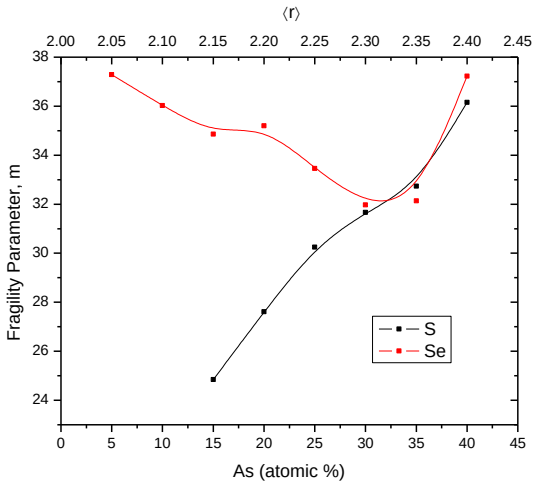


Figure 13. Variations in fragility parameter for As-Se and As-S binary chalcogenide glasses.

The fragility parameter of the arsenic selenide glass system exhibits an interesting behavior: initially, the fragility of the system decreases (ie. the viscosity curves become less steep) with the addition of low levels of arsenic, but as the glass approaches 33 molar percent of modifier (<r> = 2.33), the fragility changes directions and begins to overlap with that of the arsenic sulfide glass system. Preliminary results indicate that it is the only one of the binary chalcogenide compositions measured to display such a property; the fragility parameters of arsenic sulfide, germanium sulfide and germanium selenide all vary monotonically with modifier concentration. These results suggest that there is a fundamental change in the atomic-level network topology in the arsenic selenide series that does not occur in the other binary chalcogenides.

**2.6 Thermo-optic Behavior**

The variation in the index of refraction of a chalcogenide glass with a change in temperature is described as thermo-optic behavior, and is an extremely important, and often overlooked, aspect of infrared optical design. The induced change in refractive index is due to the thermal excitation of phonons (and electrons in some cases), and can be either positive or negative in sign depending on the composition of the glass. A positive index change in response to an applied thermal load is responsible for such phenomena as thermal lensing, self-focusing and laser damage (at high intensities), and spectral instabilities in laser resonators [54]. Despite its importance, this thermal phenomenon has received less study than the properties discussed in proceeding sections both because the instrumentation for measuring the thermo-optic coefficient as a function of wavelength is underdeveloped in the infrared, and because, as a weak optical phenomenon, it only begins to impact device design when high-precision optics are necessary [55].

The thermo-optic coefficient (dn/dT) can be measured with a prism coupling setup with an attached hot stage. A schematic of such a prism coupling measurement is shown in Figure 14. The chalcogenide glass sample is used as a substrate, and pressed in optical contact with a prism having a well-characterized

index dispersion and dn/dT. The refractive index of the chalcogenide glass at a given wavelength and temperature is measured by launching laser light of appropriate wavelength into the prism. The prism and substrate are then rotated until the incident beam is coupled from the prism into the substrate (seen as a drop in the intensity of the refracted beam); the coupling condition is dependent on the index of the substrate, that of the prism and the angle of refraction, and knowledge of the latter two enables precise calculation of the former.

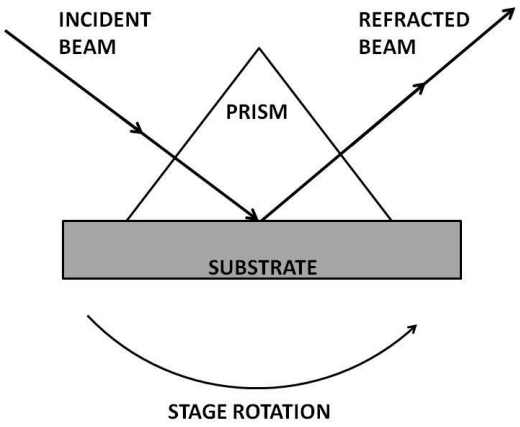


Figure 14. Schematic of a prism coupling system used to measure dn/dT

The attached hot stage can be used to heat the prism and substrate and thus measure the change in index as a function of temperature, dn/dT, at the incident wavelength. A major difficulty in accurately characterizing the thermo-optic coefficient in chalcogenide glasses is in acquiring data at a sufficient number of visible and infrared wavelengths to allow a reasonable fit for the theoretical models [56]. Changes in the refractive index as a function of both wavelength and temperature for crystalline germanium [57] and a germanium-containing chalcogenide glass are shown in Figure 15. The refractive index of the germanium crystal is a stronger function of temperature than that of the chalcogenide glass, however, this is not the case for all compositions, and in some cases the value of dn/dT can even be negative.

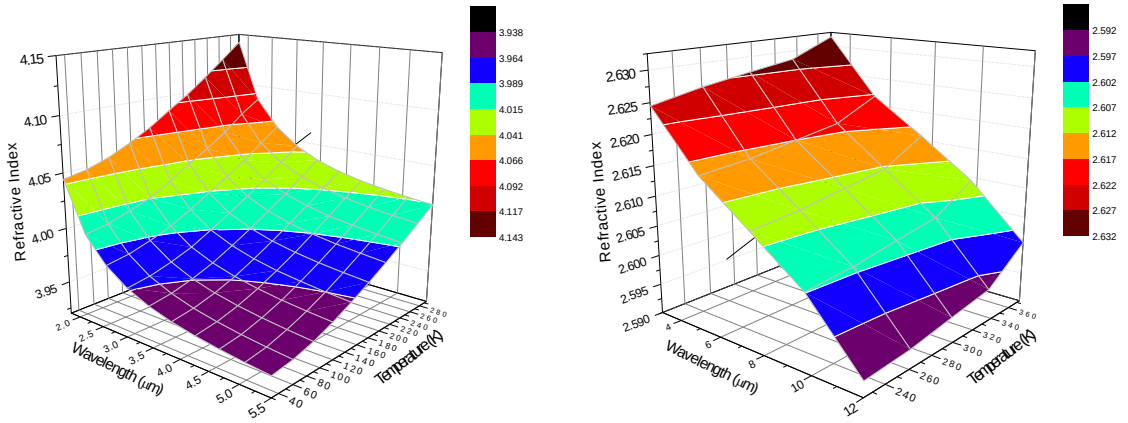


Figure 15. Variation in refractive index with wavelength and temperature for crystalline germanium (left) and a germanium-containing chalcogenide glass (right)

## 2.7 Conclusions and Future Directions

Chalcogenide glasses possess a wide range of properties which make them very attractive for fundamental research and technological development. In this chapter we have presented an overview of their thermal properties, and how these properties emerge from the material's atomic structure and impact their hot-forming ability. We have turned our focus on the standard thermal analysis techniques commonly used in glass science (differential scanning calorimetry, thermogravimetry, thermomechanical analysis and various viscometric techniques), and discussed briefly the viscoelastic and thermo-optic behaviors of the chalcogenide glasses and their impact on device design and fabrication. Specifically, an attempt was made, in binary and ternary chalcogenide systems, to reveal the composition dependence of thermal properties as a function of modifier elements content or average coordination numbers. Though similar trends occasionally arise from direct system-to-system comparisons, no global pattern enclosing the S-, Se- and Te-based glasses emerges, even in the simplest binary cases. Together, these thermal analysis techniques give precious insight into the response of the chalcogenide glasses with temperature: they contribute to measuring the characteristic thermodynamic transitions of the analytes, and give information on the kinetics underlying crystallization. Ultimately they allow the prediction, critical from a technological standpoint, of phenomena such as phase separation, vaporization, or deformation. At a fundamental level, the gathered information yields essential understanding of the structural arrangement of chalcogenide, and how it affects their thermo-mechanical, optical and electrical properties.

Thermal analysis of chalcogenide glasses has proceeded from the tools and methodology inherited from the study of other systems, mainly silica. However chalcogenide exhibit specific features (steep viscosity curves, oxidation, vaporization and associated mass changes, shift of the spectral window in the infrared), and span a variety of final product configurations, which yield particular challenges. The thermal drawing of chalcogenides into fibers for instance remains largely semi-empirical because of the lack of real-time information on the behavior of the system, especially at the bottom-neck zone, while being simultaneously subjected to heating and tension. The demonstration of the co-drawing of composite structures made of a set of materials (metal, polymer and chalcogenides) with disparate viscoelastic properties reinforces this assessment [28]. Phase-change materials, which constitute another exiting area of research for chalcogenide glasses [58], encounter similar analytical limitations. These materials, inherently unstable, require multi-layer depositions to reach their target thicknesses. This makes the in-situ probing of their glass and crystal phases impractical and leads researchers to rely heavily on indirect measurements and extrapolation. The investigation of chalcogenides would then certainly benefit from the development of dedicated in-depth, real-time analytical instrumentation; however we expect that the deepest (r)evolution in the future of chalcogenide glass development will proceed from the spectacular progress enabled by computer microprocessors. Already, robust and ergonomic modeling software is spreading in laboratories worldwide to assist in predicting thermal materials behavior and to support experimental studies.

Though part of our daily life, the true nature of the glassy state remains enigmatic. Emblematically, the glass transition temperature, the thermal signature of the glassy state, still lacks a well-accepted theoretical development. Chalcogenide glasses are complex systems where chemistry, kinetic, thermodynamic and atomic-level network mechanics intimately intertwine. It is of the utmost importance, by coupling experimental and modeling efforts, to untangle these microscopic-scale parameters dictating the material's macroscopic properties. Chalcogenides are already extensively used in night vision systems, thermal sensing and monitoring, high-power delivery fibers [44], photonic devices [59], data storage [58], and new applications are constantly emerging (holography [60], metamaterials

[61]). Further mastery of their properties would yield the promise of an even brighter future for this fascinating class of materials, an exciting challenge for the glass science community.

### 2.8 Additional Resources

Here is a series of lectures we recommend for the ones interested in chalcogenide glasses and their applications, and the thermal properties of the amorphous materials:

- B. J. Eggleton, B. Luther-Davies, K. Richardson 'Chalcogenide photonics' Nat. Photonics *5* **(2011)** 141–148
- A. Zakery, S.R. Elliott 'Optical properties and applications of chalcogenide glasses: a review', Jr. of Non-Crystal. Solids 330 (2003) 1–12
- D. Lezal 'Chalcogenide Glasses - Survey and progress', Jr of Optoelect. and Adv. Mat. 5 (2003) 23 - 34
- B. Bureau, X-H. Zhang, F. Smektala, J-L. Adam, J. Troles, H-L. Ma, C. Boussard-Pledel, J. Lucas, P. Lucas, - D. LeCoq, M. R. Riley, J. H. Simmons, "Recent advances in chalcogenide glasses" Jr. Non-Cryst. Solids *345* **(2004)** 276-283
- X. Gai, T. Han, A. Prasad, S. Madden, D-Y. Choi, R. Wang, D. Bulla, B. Luther-Davies 'Progress in optical waveguides fabricated from chalcogenide glasses' Optics Express 18 (2010) 26635-46
- A large body of work about the glass transition temperature and its modeling as been summarized in the excellent review from Berthier and Biroli [62].

### REFERENCES CITED


1. "http://www.sciglassweb.com/", retrieved 2011.
2. P. G. Debenedetti and F. H. Stillinger, "Supercooled liquids and the glass transition," Nature **410**, 259-267 (2001).
3. K. Shportko, S. Kremers, M. Woda, D. Lencer, J. Robertson, and M. Wuttig, "Resonant bonding in crystalline phase-change materials," Nature Materials **7**, 653-658 (2008).
4. F. Sciortino, W. Kob, and P. Tartaglia, "Inherent structure entropy of supercooled liquids," Phys. Rev. Lett. **83**, 3214-3217 (1999).
5. Y. Cai and M. F. Thorpe, "Floppy modes in network glasses," Physical Review B **40**, 10535-10542 (1989).
6. J. C. Phillips and M. F. Thorpe, eds., *Phase transitions and self-organization in electronic and molecular networks* (Springer, 2001).
7. J. H. Gibbs and E. A. DiMarzio, "Nature of the Glass Transition and the Glassy State," J. Chem. Phys. **28**, 373 (1958).
8. E. A. DiMarzio and J. H. Gibbs, "Glass temperature of copolymers," J. Polymer Chem. **40**, 121-131 (1959).
9. A. N. Sreeram, D. R. Swiler, and A. K. Varshneya, "Gibbs-DiMarzio equation to describe the glass-transition temperature trends in multicomponent chalcogenide glasses," J. Non-Cryst. Solids **127**, 287-297 (1991).
10. R. Kerner and M. Micoulaut, "On the glass transition temperature in covalent glasses," J. Non-Cryst. Solids **210**, 298-305 (1997).
11. J. C. Phillips and M. F. Thorpe, "Constraint theory, vector percolation and glass-formation," Solid State Commun. **53**, 699-702 (1985).
12. M. F. Thorpe, D. J. Jacobs, M. V. Chubynsky, and J. C. Phillips, "Self-organization in network glasses," J. Non-Cryst. Solids **266**, 859-866 (2000).

13. P. Boolchand, X. Feng, and W. J. Bresser, "Rigidity transitions in binary Ge-Se glasses and the intermediate phase," J. Non-Cryst. Solids **293**, 348-356 (2001).
14. P. Boolchand, D. G. Georgiev, and B. Goodman, "Discovery of the intermediate phase in chalcogenide glasses," Journal of Optoelectronics and Advanced Materials **3**, 703-720 (2001).
15. M. Popescu, "Disordered chalcogenide optoelectronic materials: Phenomena and applications," Journal of Optoelectronics and Advanced Materials **7**, 2189-2210 (2005).
16. K. Tanaka, "Photoinduced fluidity in chalcogenide glasses," C. R. Chim. **5**, 805-811 (2002).
17. J. Rocca, M. Erazu, M. Fontana, and B. Arcondo, "Crystallization process on amorphous GeTeSb samples near to eutectic point Ge(15)Te(85)," J. Non-Cryst. Solids **355**, 2068-2073 (2009).
18. G. Guery, "Influence Of Iso-Structural Substitutions On Properties Of Ge(As,Sb)(S,Se) Glasses," (Clemson University, Clemson, 2010).
19. S. Saraswat and S. S. S. Kushwaha, "Specific heat studies in a-Se and a-Se(90)M(10) (M = In, Sb, Te) alloys," Journal of Thermal Analysis and Calorimetry **96**, 923-927 (2009).
20. A. K. Varshneya, *Fundamentals of inorganic glasses* (Academic Press, 1993).
21. J. D. Musgraves, P. Wachtel, S. Novak, J. Wilkinson, and K. Richardson, "Composition dependence of the viscosity and other physical properties in the arsenic selenide glass system," Journal of Applied Physics **110**(2011).
22. ASTM, "C-1351M ".
23. ASTM, "C-1350M ".
24. ASTM, "C338."
25. L. Brilland, F. Smektala, G. Renversez, T. Chartier, J. Troles, T. N. Nguyen, N. Traynor, and A. Monteville, "Fabrication of complex structures of Holey Fibers in chalcogenide glass," Opt. Express **14**, 1280-1285 (2006).
26. T. M. Monro, Y. D. West, D. W. Hewak, N. G. R. Broderick, and D. J. Richardson, "Chalcogenide holey fibres," Electron. Lett. **36**, 1998-2000 (2000).
27. S. D. Savage, C. A. Miller, D. Furniss, and A. B. Seddon, "Extrusion of chalcogenide glass preforms and drawing to multimode optical fibers," J. Non-Cryst. Solids **354**, 3418-3427 (2008).
28. A. F. Abouraddy, M. Bayindir, G. Benoit, S. D. Hart, K. Kuriki, N. Orf, O. Shapira, F. Sorin, B. Temelkuran, and Y. Fink, "Towards multimaterial multifunctional fibres that see, hear, sense and communicate," Nature Materials **6**, 336-347 (2007).
29. D. H. Cha, H. J. Kim, H. S. Park, Y. Hwang, J. H. Kim, J. H. Hong, and K. S. Lee, "Effect of temperature on the molding of chalcogenide glass lenses for infrared imaging applications," Applied Optics **49**, 1607-1613 (2010).
30. H. Niciu, M. Popescu, A. Velea, A. Lorinczi, A. Manea, D. Niciu, and M. Lazarescu, "Moulding procedure for the preparation of infrared glassy microlenses and prisms based on arsenic sulphide chalcogenide glass," Chalcogenide Letters **7**, 625-629 (2010).
31. U. Fotheringham, M. Garsche-Andres, and E. Holzel, "Low temperature relaxation effects: Measurement with a double-microscope and relevance for glasses for flat display panels," Glass Sci Technol.-Glastech. Ber. **73**, 400-409 (2000).
32. B. Ananthasayanam, P. Joseph, V. Blouin, D. Cler, S. Gaylord, L. Petit, K. Richardson, M. Stairiker, and M. Tardiff, "Final shape of precision molded optics: Part I – Computational approach, material definition and the effect of lens shape," J. Thermal Stresses **in press**(2011).
33. B. Ananthasayanam, P. Joseph, V. Blouin, D. Cler, S. Gaylord, L. Petit, K. Richardson, M. Stairiker, and M. Tardiff, "Final shape of precision molded optics: Part II – Validation and sensitivity to material properties and process parameters," J. Thermal Stresses **in press**(2011).
34. S. Gaylord, B. Ananthasayanam, B. Tincher, L. Petit, C. Cox, U. Fotheringham, P. Joseph, and K. Richardson, "Thermal and Structural Property Characterization of Commercially Moldable Glasses," Journal of the American Ceramic Society **93**, 2207-2214 (2010).

35. T. Clopeau, A. Farina, A. Fasano, and A. Mikelic, "Asymptotic equations for the terminal phase of glass fiber drawing and their analysis," Nonlinear Anal.-Real World Appl. **11**, 4533-4545 (2010).
36. S. Danto, C. Houizot, C. Boussard-Pledel, X. H. Zhang, F. Smektala, and J. Lucas, "A new family of far IR transmitting glasses in the Ga-Ge-Te system for space applications," Adv. Funct. Mater. **16**, 1847 (2006).
37. T. D. Engeness, M. Ibanescu, S. G. Johnson, O. Weisberg, M. Skorobogatiy, S. Jacobs, and Y. Fink, "Dispersion tailoring and compensation by modal interactions in OmniGuide fibers," Opt. Express **11**, 1175-1196 (2003).
38. J. Hu, C. R. Menyuk, L. B. Shaw, J. S. Sanghera, and I. D. Aggarwal, "Maximizing the bandwidth of supercontinuum generation in As(2)Se(3) chalcogenide fibers," Opt. Express **18**, 6722-6739 (2010).
39. J. D. Shephard, W. N. MacPherson, R. R. J. Maier, J. D. C. Jones, D. P. Hand, M. Mohebbi, A. K. George, P. J. Roberts, and J. C. Knight, "Single-mode mid-IR guidance in a hollow-core photonic crystal fiber," Opt. Express **13**, 7139-7144 (2005).
40. M. El-Amraoui, G. Gadret, J. C. Jules, J. Fatome, C. Fortier, F. Desevedavy, I. Skripatchev, Y. Messaddeq, J. Troles, L. Brilland, W. Gao, T. Suzuki, Y. Ohishi, and F. Smektala, "Microstructured chalcogenide optical fibers from As(2)S(3) glass: towards new IR broadband sources," Opt. Express **18**, 26655-26665 (2010).
41. M. Asobe, T. Ohara, I. Yokohama, and T. Kaino, "Low power all-optical switching in a nonlinear optical loop mirror using chalcogenide glass fibre," Electron. Lett. **32**, 1396-1397 (1996).
42. R. E. Slusher, G. Lenz, J. Hodelin, J. Sanghera, L. B. Shaw, and I. D. Aggarwal, "Large Raman gain and nonlinear phase shifts in high-purity As2Se3 chalcogenide fibers," J. Opt. Soc. Am. B-Opt. Phys. **21**, 1146-1155 (2004).
43. S. J. Madden, D. Y. Choi, D. A. Bulla, A. V. Rode, B. Luther-Davies, V. G. Ta'eed, M. D. Pelusi, and B. J. Eggleton, "Long, low loss etched As2S3 chalcogenide waveguides for all-optical signal regeneration," Opt. Express **15**, 14414-14421 (2007).
44. B. Bureau, X. H. Zhang, F. Smektala, J. L. Adam, J. Troles, H. L. Ma, C. Boussard-Pledel, J. Lucas, P. Lucas, D. Le Coq, M. R. Riley, and J. H. Simmons, "Recent advances in chalcogenide glasses," J. Non-Cryst. Solids **345**, 276-283 (2004).
45. M. Bayindir, F. Sorin, A. F. Abouraddy, J. Viens, S. D. Hart, J. D. Joannopoulos, and Y. Fink, "Metal-insulator-semiconductor optoelectronic fibres," Nature **431**, 826-829 (2004).
46. S. Egusa, Z. Wang, N. Chocat, Z. M. Ruff, A. M. Stolyarov, D. Shemuly, F. Sorin, P. T. Rakich, J. D. Joannopoulos, and Y. Fink, "Multimaterial piezoelectric fibres," Nature Materials **9**, 643-648 (2010).
47. A. F. Abouraddy, O. Shapira, M. Bayindir, J. Arnold, F. Sorin, D. S. Hinczewski, J. D. Joannopoulos, and Y. Fink, "Large-scale optical-field measurements with geometric fibre constructs," Nature Materials **5**, 532-536 (2006).
48. S. Danto, F. Sorin, N. D. Orf, Z. Wang, S. A. Speakman, J. D. Joannopoulos, and Y. Fink, "Fiber Field-Effect Device Via In Situ Channel Crystallization," Advanced Materials **22**, 4162-+ (2010).
49. G. S. Fulcher, "Analysis of recent measurements of the viscosity of glass," J. Am. Ceram. Soc. **8**, 339-355 (1925).
50. J. C. Mauro, Y. Yue, A. J. Ellison, P. K. Gupta, and D. C. Allan, "Viscosity of glass-forming liquids," Proceedings of the National Academy of Sciences of the United States of America **106**, 19780-19784 (2009).
51. L. Petit, N. Carlie, R. Villeneuve, J. Massera, M. Couzi, A. Humeau, G. Boudebs, and K. Richardson, "Effect of the substitution of S for Se on the structure and non-linear optical properties of the glasses in the system Ge0.18Ga0.05Sb0.07S0.70-Se-x(x)," J. Non-Cryst. Solids **352**, 5413-5420 (2006).

52. M. D. Ediger, C. A. Angell, and S. R. Nagel, "Supercooled liquids and glasses," Journal of Physical Chemistry **100**, 13200-13212 (1996).
53. V. N. Novikov, Y. Ding, and A. P. Sokolov, "Correlation of fragility of supercooled liquids with elastic properties of glasses," Phys. Rev. E **71**, 12 (2005).
54. J. Nishii, S. Morimoto, I. Inagawa, R. Iizuka, T. Yamashita, and T. Yamagishi, "Recent advances and trends in chalcogenide glass-fiber technology - A review," J. Non-Cryst. Solids **140**, 199-208 (1992).
55. J. Mangin, G. Mennerat, and P. Villeval, "Thermal expansion, normalized thermo-optic coefficients, and condition for second harmonic generation of a Nd:YAG laser with wide temperature bandwidth in RbTiOPO4," J. Opt. Soc. Am. B-Opt. Phys. **28**, 873-881 (2011).
56. N. Cherroret, A. Chakravarty, and A. Kar, "Temperature-dependent refractive index of semiconductors," Journal of Materials Science **43**, 1795-1801 (2008).
57. G. Hawkins and R. Hunneman, "The temperature-dependent spectral properties of filter substrate materials in the far-infrared (6-40 mu m)," Infrared Physics & Technology **45**, 69-79 (2004).
58. M. Wuttig and N. Yamada, "Phase-change materials for rewriteable data storage (vol 6, pg 824, 2007)," Nature Materials **6**, 1004-1004 (2007).
59. B. J. Eggleton, B. Luther-Davies, and K. Richardson, "Chalcogenide photonics," Nat. Photonics **5**, 141-148 (2011).
60. J. Teteris and M. Reinfelde, "Application of amorphous chalcogenide semiconductor thin films in optical recording technologies," Journal of Optoelectronics and Advanced Materials **5**, 1355-1360 (2003).
61. E. Semouchkina, D. H. Werner, G. B. Semouchkin, and C. Pantano, "An infrared invisibility cloak composed of glass," Applied Physics Letters **96**(2010).
62. L. Berthier and G. Biroli, "Theoretical perspective on the glass transition and amorphous materials," Reviews of Modern Physics **83**, 587-645 (2011).